

---

# POTENTIAL OF DEEP OPERATOR NETWORKS IN DIGITAL TWIN-ENABLING TECHNOLOGY FOR NUCLEAR SYSTEMS

---

A PREPRINT

**Kazuma Kobayashi**

Nuclear, Plasma & Radiological Engineering  
University of Illinois at Urbana-Champaign  
Urbana, IL 61801, USA

**Syed Bahauddin Alam**

Nuclear, Plasma & Radiological Engineering  
University of Illinois at Urbana-Champaign  
Urbana, IL 61801, USA

August 16, 2023

## ABSTRACT

This research introduces the Deep Operator Network (DeepONet) as a robust surrogate modeling method within the context of digital twin (DT) systems for nuclear engineering. With the increasing importance of nuclear energy as a carbon-neutral solution, adopting DT technology has become crucial to enhancing operational efficiencies, safety, and predictive capabilities in nuclear engineering applications. DeepONet exhibits remarkable prediction accuracy, outperforming traditional ML methods. Through extensive benchmarking and evaluation, this study showcases the scalability and computational efficiency of DeepONet in solving a challenging particle transport problem. By taking functions as input data and constructing the operator  $G$  from training data, DeepONet can handle diverse and complex scenarios effectively. However, the application of DeepONet also reveals challenges related to optimal sensor placement and model evaluation, critical aspects of real-world implementation. Addressing these challenges will further enhance the method's practicality and reliability. Overall, DeepONet presents a promising and transformative tool for nuclear engineering research and applications. Its accurate prediction and computational efficiency capabilities can revolutionize DT systems, advancing nuclear engineering research. This study marks an important step towards harnessing the power of surrogate modeling techniques in critical engineering domains.

## 1 Introduction

A reliable and sustainable energy supply is essential to support and drive economic activity in the modern world. As the urgent need for carbon-neutral solutions becomes increasingly evident, nuclear energy is projected to assume a significant role. With the ongoing global increase in energy demands, nuclear power is poised to emerge as a critical and environmentally friendly alternative to conventional energy sources.

Furthermore, nuclear research is actively exploring novel technologies and approaches to advance the field further. Among these exciting research areas, the utilization of digital twin (DT) technology in nuclear systems has gained substantial attention. The United States Nuclear Regulatory Commission (U.S. NRC) recognizes the potential of DT technology and has identified it as a key area for future research Yadav et al. [2021]. The NRC has highlighted several potential benefits of DTs in nuclear energy applications, including increased operational efficiencies, enhanced safety and reliability, reduced errors, faster information sharing, and improved predictive capabilities Yadav et al. [2021], Kobayashi et al. [2022]. However, it is important to acknowledge that the development of DT technology for nuclear systems is still in its nascent stages, and numerous challenges must be addressed and overcome Kazuma et al. [2023]. Although when dealing with DT technology, the physical system of the real world (i.e., called "physical assets"), its replication in virtual space (i.e., called "digital replica") and the Internet of Things (IoT) technology that connects them are essential IBM, Amazon Web Services, GE Digital, Redshift by AUTODESK, and this study focuses on *modeling and simulation* technique using a digital replica.

A digital replica is created by capturing and integrating various data sources, such as sensor data, operational data, and design specifications, to generate a highly detailed and accurate representation of the physical system IBM. This

virtual replica serves multiple purposes, including monitoring, analysis, simulation, and prediction. While traditional analysis and simulation codes can fulfill these roles, it can be challenging to strike a balance between accuracy and speed, especially in systems requiring rapid analysis and response prediction.

In certain domains like nuclear reactor systems, dedicated codes are employed for analysis. However, these codes often prioritize high analysis accuracy, which can result in high computational costs. Relying solely on expensive simulations based on real-time information from various sensors installed in the reactor system and then making control decisions based on the results can lead to sluggish operator response times and, in extreme cases, potentially catastrophic nuclear accidents. This situation calls for a new approach in digital twin technology for reactor systems Rahman et al. [2022], Daniell et al. [2022, 2023] that simultaneously addresses the need for high calculation accuracy and calculation speed.

To address this challenge, this study proposes the utilization of high-fidelity data-driven surrogate modeling, employing the Deep Operator Network as a method to meet these stringent requirements. This approach aims to strike a balance between accuracy and computational efficiency. Additionally, the study includes a demonstration of modeling employing a particle transport code as a high-fidelity data generator.

Please note that this work is an extension of previously published studies Kobayashi et al. [2023a,b] by the lead author. This paper builds upon and expands the concepts and findings of those publications. In this extended version, we delve deeper into the practical application of the Deep Operator Network in nuclear engineering problems, providing additional insights and discussions. The current work also introduces new experimental data and presents further validations to reinforce the robustness of the proposed approach.

## 2 Deep operator network (DeepONet)

DeepONet, akin to neural networks, is built upon the Universal Approximation Theorem but focuses on the Universal Approximation Theorem for Operators Lu et al. [2021a], Chen and Chen [1995]. While traditional neural networks map inputs to a function space, DeepONet is designed to map information from functions to an operator that can be observed in any domain.

Suppose  $G$  is an operator which takes an input function  $u$ ; this assumption makes  $G(u)$  the output function corresponding to the input one. In the domain of  $G(u)$ , the real number at any sampling point  $y$  can be expressed as  $G(u)(y)$ . To handle an input function in calculations, it must be discretized in the input space  $V$ . In the concept of DeepONet Lu et al. [2021a], input functions are discretized by sampling at the fixed positions  $\{x_1, x_2, \dots, x_m\}$  where  $m$  represents the number of discretized points. Therefore, DeepONet can handle the two network inputs;  $[u(x_1), u(x_2), \dots, u(x_m)]^T$  and  $y \in \mathbb{R}^d$ . Based on the Universal Approximation Theorem for Operator, the operator  $G$  can be expressed by the Generalized Universal Approximation Theorem for Operator by Lu et al. [2021a], Cai et al. [2021] as follows:

$$\left| G(u)(y) - \underbrace{\langle \mathbf{g}(u(x_1), u(x_2), \dots, u(x_m)), \mathbf{f}(y) \rangle}_{\text{branch}} \right| < \epsilon \quad (1)$$

where  $\epsilon > 0$ ,  $\mathbf{g}$  and  $\mathbf{f}$  are continuous vector functions  $\mathbf{g} : \mathbb{R}^m \rightarrow \mathbb{R}^p$  and  $\mathbf{f} : \mathbb{R}^d \rightarrow \mathbb{R}^p$ ,  $\langle \cdot, \cdot \rangle$  represents the dot product in  $\mathbb{R}^p$ . The function  $\mathbf{g}$  and  $\mathbf{f}$  are replaced with neural networks. Here, the NNs that handle the input function are distinguished as "branch" and those that handle the input vector  $y \in \mathbb{R}^d$  as "trunk." Since the main topic of this study is the applied use of DeepONet, please refer to Lu et al. [2021a,b] for more detailed mathematical proof.

DeepONet employs the branch-trunk architecture, where the "branch" and "trunk" networks are subnetworks implemented using NNs Lu et al. [2021a], Goswami et al. [2022]. The trunk network deals with domain information, while the branch network encodes sensor information from the function. Internal filtering allows DeepONet to handle data efficiently. This architecture is harnessed to approximate the system's operator and the entire model is trained using loss associated with the predictions. Figure 1 illustrates the branch-trunk architecture. For a more in-depth mathematical proof, refer to Lu et al. [2021a,b].

## 3 Experiments

In order to showcase the capabilities of DeepONet, a surrogate model is constructed for calculating the 2-dimensional spatial distribution of neutron flux. The training and test datasets used for training the DeepONet model are prepared using Particle and Heavy Ion Transport code System (PHITS) version 3.24 Sato et al. [2018]. This section elaborates on the methodology employed for data generation and the simulation setup utilized in this study.

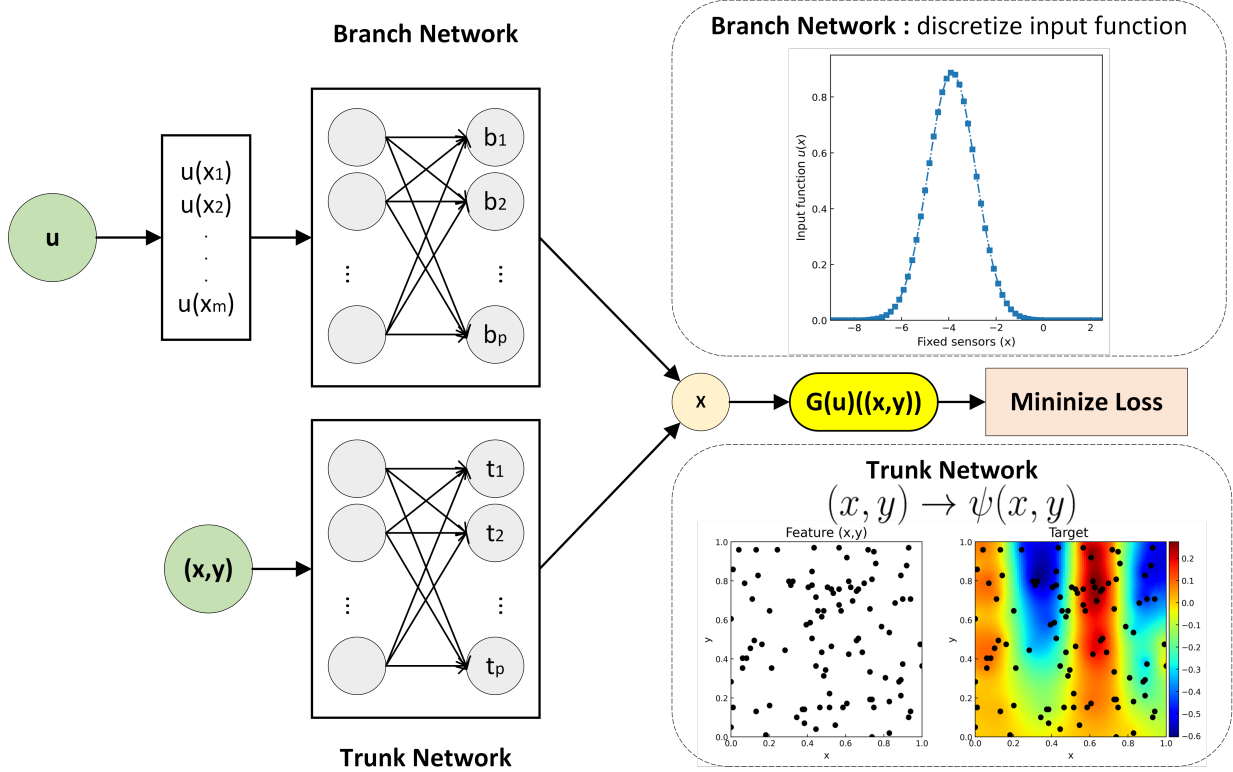


Figure 1: Illustration of DeepONet Branch-Trunk architecture Lu et al. [2021a], Kobayashi et al. [2023b]. It is an example when the input vector is composed of 2-dimension (i.e.,  $y = [x, y]$ ). The discretized input functions and input vector  $y$  are individually fed into fully-connected neural networks. Then, the dot product is computed using their network outputs.

### 3.1 Particle Transport Code

PHITS, a Monte Carlo particle transport simulation code, has the capability to accurately simulate particle transport across a wide range of energy spectra through the utilization of sophisticated nuclear reaction models and comprehensive data libraries Sato et al. [2018]. Its versatility allows for its application in various research fields, including accelerator technology, radiotherapy, space radiation, and other domains involving particle and heavy ion transport phenomena. In this study, we leverage the power of PHITS to simulate the 2D spatial distribution of neutron flux within a maze. To accomplish this, we have customized and employed the sample code provided by the PHITS Development Group as a foundation for our research. For particle transport calculations in PHITS, the definition of geometry, material, radiation sources, and the phenomenon to be analyzed, referred to as Tally, is necessitated.

#### 3.1.1 Geometry

In our simulation, a maze with concrete walls enclosing an air-filled interior is chosen as the geometry, as depicted in Figure 2 (a). During the configuration of the geometry, there is no need to specify the spatial resolution, such as the grid size, as it is a critical factor affecting the accuracy of the calculation and is determined when defining the Tally, as elucidated later.

#### 3.1.2 Material

The material densities of concrete and air are set to  $1.2 \times 10^{-3}$  g/cm and 2.2 g/cm, respectively. For each defined element, nuclear reaction cross-sections are bundled from the nuclear data library JENDL-4.0 Shibata et al. [2011]. Moreover, the detail of material compositions used in this study is provided in A.1.

### 3.1.3 Neutron Source

The simulation utilizes a Gaussian distribution neutron source. This source is characterized by independent Gaussian distributions along each component of the vector  $\mathbf{x} = [x_1, x_2, x_3]$ . Assuming independent variables, the covariance matrix  $\Sigma$  takes the form of a diagonal matrix with variances  $\sigma_j^2$  for each variable, as shown in Equation 2:

$$\Sigma = \begin{pmatrix} \sigma_1^2 & 0 & 0 \\ 0 & \sigma_2^2 & 0 \\ 0 & 0 & \sigma_3^2 \end{pmatrix}. \quad (2)$$

Here, the subscript  $j$  corresponds to the direction. Consequently, the 3-dimensional Gaussian distribution  $\phi(\mathbf{x})$  is expressed by Equation 3:

$$\phi(\mathbf{x}) = \prod_{j=1}^3 \frac{1}{\sqrt{2\pi\sigma_j^2}} \exp \left\{ -\frac{1}{2\sigma_j^2} (x_j - \mu_j)^2 \right\}. \quad (3)$$

Finally, the neutron source  $u(E, \mathbf{x})$  is defined by multiplying a peak energy  $E$  by the distribution obtained in Equation 3:

$$u(E, \mathbf{x}) = E \phi(\mathbf{x}) = E \prod_{j=1}^3 \frac{1}{\sqrt{2\pi\sigma_j^2}} \exp \left\{ -\frac{1}{2\sigma_j^2} (x_j - \mu_j)^2 \right\}, \quad (4)$$

where  $\mu_j$  represents the component of the mean vector  $\mu$ .

For every simulation, the peak energy  $E$  and mean position  $\mu_2$  are randomly generated within the ranges of  $E$  and  $y$  are defined by  $E \in (0, 1)$  in MeV and  $y \in [-9, 9]$  in cm, respectively. These values are then employed in Equation 4 to prepare the neutron source. It should be noted that the variances  $\sigma_1^2 = \sigma_2^2 = 1$ ,  $\sigma_3^2 = 0$ , and mean values  $\mu_1 = \mu_3 = 0$  remain fixed throughout the process. The possible regions of the mean position  $y$  are indicated by the red boxed area in Figure 2 (a). Figure 2 (b) shows an example of 15 randomly generated patterns of neutron sources projected onto the  $y$ -plane, which confirms that the peak energy and peak position are each a random combination.

### 3.1.4 Tally

The flux within the geometry is calculated using the [T-Track] tally. To cover potential peak energies up to 1 MeV, the energy mesh range is defined from 1 keV to 10 MeV. For spatial resolution, the geometry is divided into 80 divisions in both the  $x$ - and  $y$ -directions, ranging from  $-12$  cm to  $52$  cm, while a single division is used in the  $z$ -direction, covering a range from  $-10$  cm to  $10$  cm. This results in the definition of 6,400 sub-regions on the  $xy$ -plane and the neutron flux values are computed for each of these regions. In this calculation, a normalization factor of 1,000 is set to avoid the default per-particle normalization in PHITS, which would result in a significantly smaller value.

## 3.2 Executing the simulations

A total of 1,900 random combinations of peak energy  $E$  and the mean value of  $y$  positions are generated, and simulations are carried out for each combination. Each simulation includes  $10^5$  neutrons per batch, with a total of  $10^2$  batches per combination. This setup ensures that the relative error of the neutron flux remains below 10%.

In order to provide a comprehensive comparison between the simulation and surrogate model runtimes, it is important to include information about the computational environment. The simulations are performed on a machine running the Ubuntu 22.04 operating system, equipped with an AMD Ryzen9 3900X CPU (12 Cores/24 Threads) and 64GB DRAM (3,200 Hz). PHITS version 3.24, compiled by our group with the Intel Fortran Compiler (Intel(R) Parallel Studio XE 2020 Update 1 for Linux), is used for hybrid MPI and OpenMP parallel computing. The number of threads (or cores) to be used for OpenMP is set to 2 threads per core, and one for MPI is 11 cores. Based on the log data, the time required per simulation was  $30.54 \pm 3.76$  seconds.

## 3.3 Preprocessing

This section presents an overview of the data preprocessing methods employed to construct a surrogate model using the simulation results. The data preprocessing steps are crucial for extracting meaningful information from the input functions and preparing the data for training the DeepONet model, as described in Section 2.

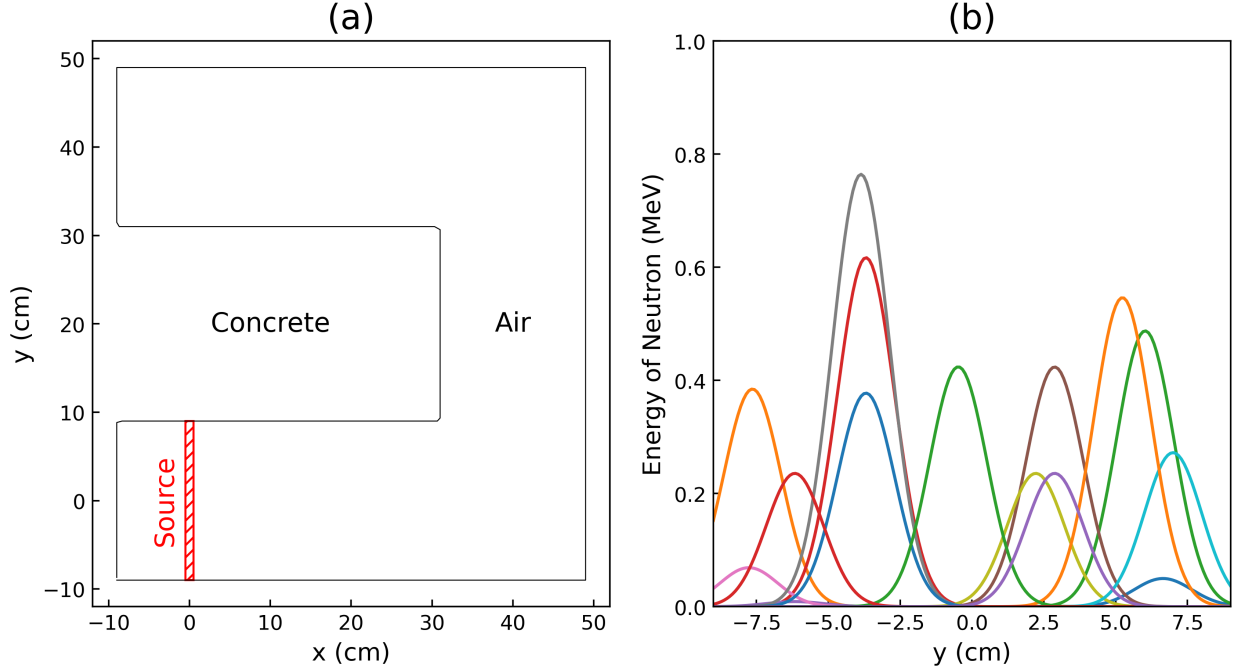


Figure 2: (a) the layout of the concrete maze used in the particle transport simulation. The maze is enclosed by concrete walls, and the interior is filled with air. The neutron source position  $y$  is randomly selected, while the  $x$  location is fixed at  $x = 0$ . (b) example of randomly generated Gaussian distribution neutron sources. The peak energy  $E$  and the Gaussian center position in the  $y$ -axis are randomly generated in each simulation run (see Section 3.1.3).

The first step involves the branch network, which is responsible for receiving the input functions and capturing their features. To effectively capture the features of the 1,900 patterns of input functions, values are sampled from Equation 4 at a set of 190 fixed positions for each neutron source. This discretization process entails sampling the continuous input functions at specific points, resulting in discrete values. Notably, the same fixed sampling positions are applied to all input functions, ensuring consistency across the dataset. Figure 3 (a) visually illustrates this sampling process.

Moving on to the trunk network, its primary role is to establish the relationship between the input features  $\mathbf{y}$  (in this case, sampling position  $(x, y)$  in 2-dimensional geometry) and the system output  $\psi(\mathbf{y})$ . In essence, the trunk network performs a conventional regression task using neural networks such as fully connected neural networks (FCN) and convolutional neural networks (CNN). By leveraging the power of NNs, the Trunk network learns the intricate patterns, correlations, and nonlinear mappings that exist between the input variables and the system output.

In order to prepare training and test datasets, the 1,900 simulation results are split into sub-datasets with a ratio of 8:2, respectively. As mentioned in Section 3.1.4, there are 6,400 pairs of  $(x, y)$  positions on the mesh and corresponding simulation results  $\psi(x, y)$  for one input function  $\phi(y)$  (i.e., neutron source). While all of these pairs can be used for surrogate model building, multiple datasets are created to compare how their number affects the model performance: randomly sampling data in 10% increments from 50% to 90% of the total 6,400 pairs. Figure 3 (b) shows the positions  $(x, y)$  on the simulation mesh when 50% of sampling.

### 3.4 DeepONet Model

The desired function of a DeepONet model is to obtain the operator that maps between the distribution of neutron source and the 2-dimensional spatial distribution of neutron flux in the maze. In this case, the operator  $G$  can be noted as  $G : u(E, \mathbf{y}) \mapsto \psi(\mathbf{y})$ . To build the model, DeepONet network architecture, model training, and evaluation methods are provided in this section. The implementation of DeepONet is done using the scientific machine learning library DeepXDE Lu et al. [2021b].

DeepONet utilizes fully connected neural networks for both the branch and trunk networks. The branch network has a layer size of [190, 80, 80], while the trunk network has a layer size of [2, 80, 80] to accommodate the two-dimensional input  $(x, y)$ .

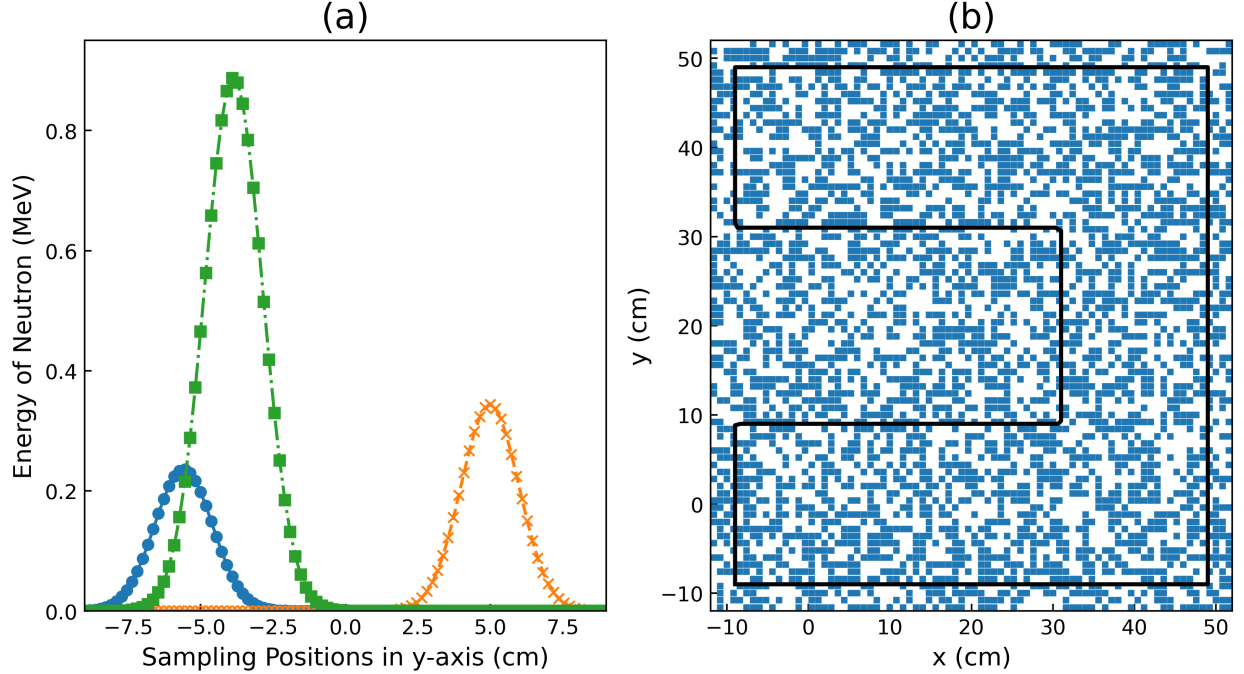


Figure 3: (a) Illustration of sampling from input functions at fixed positions, and (b) Sampling positions of simulation output on an  $80 \times 80$  mesh. The blue-colored cells indicate the positions  $(x, y)$  used for training the DeepONet model.

During the training process, the Adam optimization algorithm is employed as the optimization method. The mean  $L^2$  relative error serves as the evaluation metric to assess the model’s performance. The model is trained for 10,000 iterations with a learning rate of 0.001. The learning rate determines the step size during gradient descent and influences the convergence speed and accuracy of the training process. These choices of optimization algorithm, evaluation metric, and learning rate are consistent across all training datasets, ensuring a fair and comparable evaluation of the models.

To evaluate the performance of DeepONet models trained on each training dataset, four indices are employed: the  $R^2$  score, root-mean-squared deviation (RMSE), mean absolute error (MAE), and the ratio of RMSE to MAE (RMSE/MAE). These indices provide insights into the accuracy, precision, and general performance of the trained models.

## 4 Results

### 4.1 Overall performance of the DeepONet models

The evaluation of DeepONet models using different datasets demonstrated their performance on the test dataset in terms of  $R^2$  score, RMSE, MAE, and RMSE/MAE, with Table 1 presenting the mean and standard deviation of each metric. The results revealed that larger training datasets led to improved model performance. Even with the smallest dataset, the DeepONet models achieved impressive results, with  $R^2$  values reaching 0.99 and RMSE and MAE staying within 10%. For more detailed metrics for all model test data, please refer to Appendix B.

Ideally, a well-constructed model should capture the general trends in the data, with only random noise following a normal distribution being represented as errors. In such cases, the ratio of RMSE to MAE should be close to 1.253. However, the observed ratio of approximately 1.53 in all models indicates the presence of data points significantly deviating from the model predictions, suggesting the influence of outliers.

To address this issue, two potential solutions are considered. Firstly, the removal of outliers from the training dataset can improve model generalization and performance by focusing on representative data. Secondly, hyperparameter tuning allows the DeepONet model to adapt more effectively to the dataset’s complexities, fine-tuning its performance.

Combining both approaches can lead to a more robust and accurate DeepONet model, enabling reliable predictions even in the presence of challenging data points. Implementing these improvements will enhance the model’s effectiveness and applicability, making it a valuable tool in the context of this study.

Table 1: Performance of DeepONet models evaluated with  $R^2$ , RMSE, MAE, and RMSE/MAE. The details of datasets are described in Section 3.3.

Dataset	Metrics			
	$R^2(\times 10^{-1})$	RMSE ( $\times 10^{-2}$ )	MAE ( $\times 10^{-2}$ )	RMSE/MAE
Set1 (50%)	$9.93 \pm 0.02$	$6.61 \pm 1.49$	$4.27 \pm 1.20$	$1.56 \pm 0.13$
Set2 (60%)	$9.93 \pm 0.02$	$6.57 \pm 1.47$	$4.47 \pm 1.22$	$1.49 \pm 0.10$
Set3 (70%)	$9.93 \pm 0.02$	$6.43 \pm 1.35$	$4.17 \pm 1.15$	$1.56 \pm 0.12$
Set4 (80%)	$9.95 \pm 0.02$	$5.71 \pm 1.40$	$3.84 \pm 1.20$	$1.51 \pm 0.12$
Set5 (90%)	$9.96 \pm 0.02$	$5.14 \pm 1.33$	$3.45 \pm 1.16$	$1.52 \pm 0.12$

## 4.2 Comparisons with FCN and CNN

This section compares the model’s performance trained with Set1 on the test data against FCN and CNN. As mentioned earlier, DeepONet takes functions as inputs, and the model test evaluates its response to unseen input functions. In this study, 380 test input functions were provided to the model, and the obtained model outputs were compared to the true values. The same metrics used in the previous section were calculated for each input function.

To distinguish each input function, identification numbers (Test ID) were assigned from 1 to 380. Notably, when Test ID 23 and 18 were used, the DeepONet model demonstrated the highest and lowest  $R^2$  values, respectively. To compare with conventional ML methods, FCNs and CNNs were trained on these two cases, and the metrics were computed similarly. For more detailed information on the network architectures of FCNs and CNNs in these cases and the parameters used during training, please refer to Appendix C.

The calculation results are summarized in Table 2. In both cases of Test IDs 23 and 18, the DeepONet model outperformed FCN and CNN in terms of  $R^2$  score, RMSE, and MAE. Particularly, for Test ID 23, the DeepONet model exhibited significantly better performance with RMSE and MAE values superior by order of magnitude compared to the other models. Additionally, in the challenging case of Test ID 18, where FCN and CNN struggled to build accurate models, DeepONet achieved an impressive  $R^2$  value exceeding 0.9, while its RMSE and MAE demonstrated several times better performance than the other models. However, it is noteworthy that the ratio of RMSE to MAE for DeepONet was relatively higher than that of FCN and CNN when comparing the models.

Table 2: Performances of DeepONet model (Set1), FCN, and CNN.

Test ID	Model	Metrics			
		$R^2(\times 10^{-1})$	RMSE ( $\times 10^{-2}$ )	MAE ( $\times 10^{-2}$ )	RMSE/MAE
Highest (ID: 23)	DeepONet	9.97	4.77	3.06	1.56
	FCN	9.07	25.20	19.30	1.31
	CNN	9.03	25.70	19.43	1.32
Lowest (ID: 18)	DeepONet	9.79	17.42	12.95	1.35
	FCN	5.25	84.65	72.02	1.18
	CNN	4.26	93.03	80.99	1.15

In addition to quantitative model performance considerations, confirming the reproducibility of physical phenomena is crucial. In this study, we modeled the spatial distribution of neutron flux using the neutron source distribution in a two-dimensional space as an input function ( $G : u(E, \mathbf{y}) \mapsto \psi(\mathbf{y})$ ). Since the system under consideration lacks fissile material, the Gaussian center position of the neutron source distribution is expected to have the highest value. Based on this fact, we compared the predictions of DeepONet, FCN, and CNN models.

Figure 4 presents the ground truth from the simulation, along with the predictions of DeepONet, FCN, and CNN for Test ID 23. As expected, the highest values are obtained at the Gaussian center position of the neutron source (Figure 4 (a)). The DeepONet model can reproduce the overall distribution of neutron flux, although the peak value at the Gaussian center position is estimated to be small (Figure 4 (b)). In contrast, FCN and CNN fail to accurately reproduce both the Gaussian center location and the overall neutron distribution prediction (Figures 4 (c) and (d)).

Figure 5 shows the ground truth from the simulation and the predictions of DeepONet, FCN, and CNN for Test ID 18. The DeepONet model is capable of reproducing the overall distribution of neutron flux, although the Gaussian center position is slightly blurred (Figure 5 (b)). On the other hand, FCN and CNN models do not accurately reproduce the neutron flux distribution, especially in the upper-left regions farthest from the neutron source (Figures 5 (c) and 5 (d)).

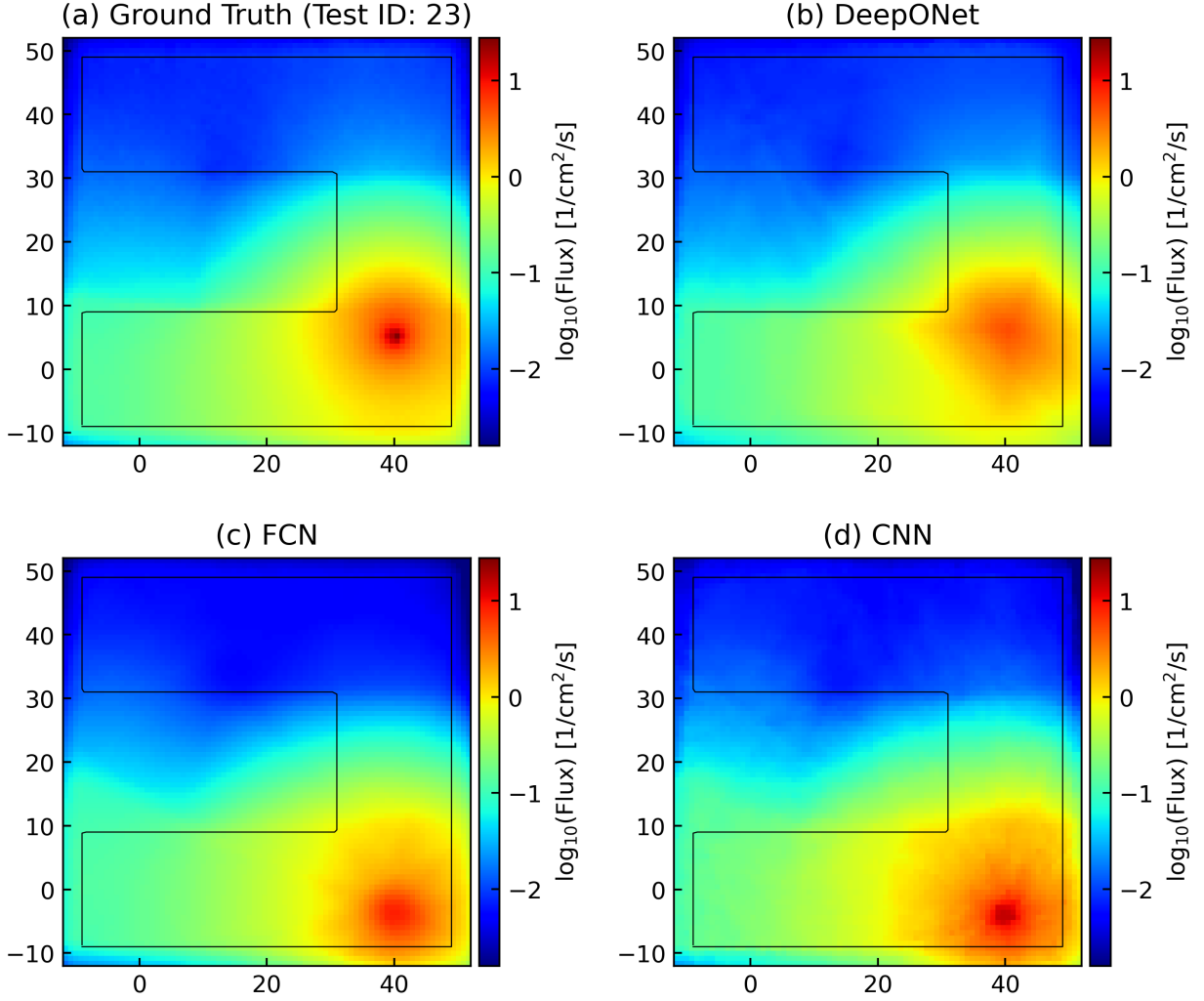


Figure 4: Comparisons between the ground truth, DeepONet, FCN, and CNN predictions for the Test ID of 23.

Notably, in this test case, the neutron flux is overestimated relative to the true value, which could lead to potentially hazardous situations from a radiation protection perspective if underestimated.

Overall, these findings underscore the ability of the DeepONet model better to capture the intricate spatial distribution of neutron flux compared to FCN and CNN models, showcasing its potential for reliable and accurate predictions in nuclear engineering applications.

## 5 Discussions

The study demonstrates the power of DeepONet, which takes functions as input data and constructs operator  $G$  in the system using training data. Notably, the prediction accuracy of DeepONet matches or surpasses that of conventional ML methods like FCN and CNN. The use of fixed sensors to extract features from input functions and their integration into the model through a branch network is a compelling concept. Training the model with historical data or high-confidence simulations allows it to handle diverse scenarios, including various accidents in the process.

An essential advantage of DeepONet, shared by many ML-based surrogate models, is its remarkably fast execution speed compared to conventional simulations. While a PHITS simulation took about 30 seconds (see Section 3.2), DeepONet performed the task in just 0.02 seconds. This remarkable speed makes DeepONet a potent modeling method for digital twin systems, enabling real-time predictions based on data from sensors installed on physical assets.



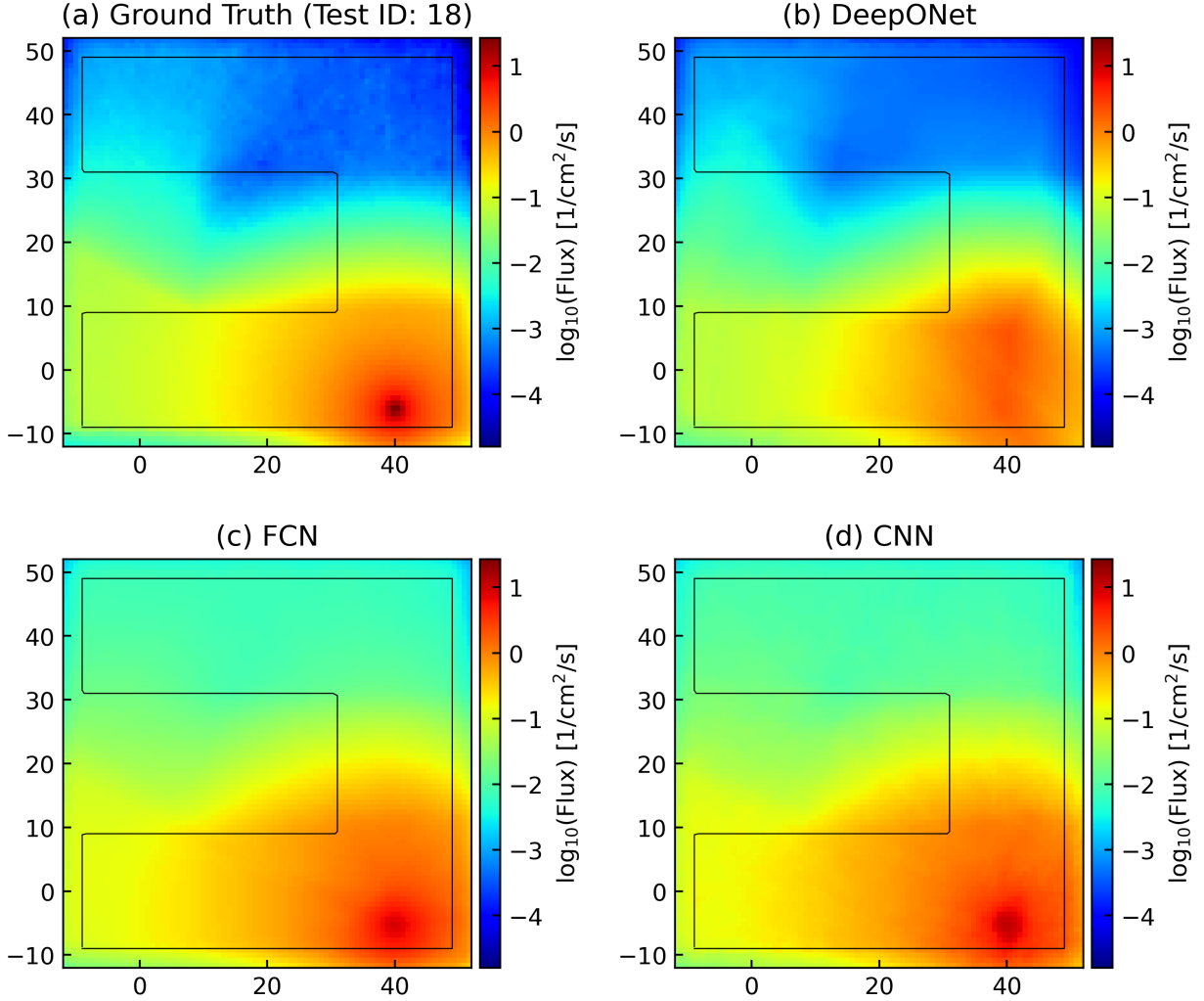


Figure 5: Comparisons between the ground truth, DeepONet, FCN, and CNN predictions for the Test ID of 18.

To further enhance the application of DeepONet, two important issues must be addressed. Firstly, understanding the impact of fixed sensors' number and location on model performance is crucial, considering the limited installation possibilities in harsh environments like nuclear power systems. Optimizing sensor placement and quantity under such constraints will be necessary for accurate and reliable modeling. Secondly, evaluating the DeepONet model requires attention. While overall metrics may indicate excellent performance, certain input functions might produce spurious predictions (see Section 4.1 and Section 4.2). Improving the model evaluation process, including hyperparameter tuning, is necessary to ensure robust and dependable predictions in all scenarios.

By addressing these challenges, DeepONet can be further optimized for digital twin systems, enhancing its potential to predict and analyze current and future systems based on real-time data from physical assets' sensors. This advancement opens new possibilities for various engineering applications, including nuclear engineering and beyond.

## 6 Conclusions

In conclusion, this research has highlighted the significant potential of DeepONet as a powerful surrogate modeling method in the context of digital twin (DT) systems for nuclear engineering. The utilization of DeepONet allows for the accurate prediction of complex behaviors and spatial distributions of neutron flux, surpassing the performance of conventional ML methods like FCN and CNN. Its ability to handle functions as input data and construct operator  $G$  from training data makes it a valuable tool for capturing the intricate behavior of nuclear systems.

Through extensive benchmarking and evaluation, DeepONet showcased remarkable prediction accuracy and computational efficiency. It demonstrated consistent improvement in performance with increasing training datasets, making it a versatile and scalable solution for various nuclear engineering applications. The speed of execution, significantly faster than traditional simulations, positions DeepONet as a promising method to enable real-time predictions based on sensor data from physical assets.

While DeepONet shows great promise, the study also sheds light on challenges that need further investigation. The impact of fixed sensors and the optimal sensor placement for improved model performance requires careful consideration, given the constraints in harsh operating environments like nuclear power systems. Additionally, developing more effective model evaluation methods is crucial to ensure reliable predictions and robustness.

Overall, this research contributes valuable insights into the advancement of digital twin technology in nuclear engineering. By harnessing the capabilities of DeepONet, researchers and operators can enhance the safety, efficiency, and reliability of nuclear systems, paving the way toward a sustainable and carbon-neutral energy future. As digital twin systems continue to evolve and mature, DeepONet is a promising and innovative approach to revolutionizing nuclear engineering research and applications.

## Acknowledgement

The computational part of this work was supported in part by the National Science Foundation (NSF) under Grant No. OAC-1919789.

## A PHITS Input

### A.1 Material Composition

The compositions of air and concrete employed in this study are presented in Tables 3 and 4. In PHITS, materials can be defined using either atomic ratio or mass ratio. The identification of nuclei can be expressed in terms of the number of protons  $Z$  and atomic number  $A$  using the following formula:

$$\text{Name of Nuclide} = Z \times 1000 + A. \quad (5)$$

Table 3: Composition of air

Nuclide	Composition <sup>1</sup>
7014	78.08
8016	20.95
Density (g/cm <sup>3</sup> )	$1.21 \times 10^{-3}$

<sup>1</sup> atomic ratio of air

Table 4: Composition of concrete

Nuclide	Composition <sup>2</sup>
1001	0.011
11023	0.043
13027	0.145
16032	0.002
20040	0.197
26056	0.085
8016	1.05
12024	0.034
14028	0.592
19039	0.035
22048	0.006
Density (g/cm <sup>3</sup> )	2.2

<sup>2</sup> mass ratio of concrete

## B Overall performance of the DeepONet models

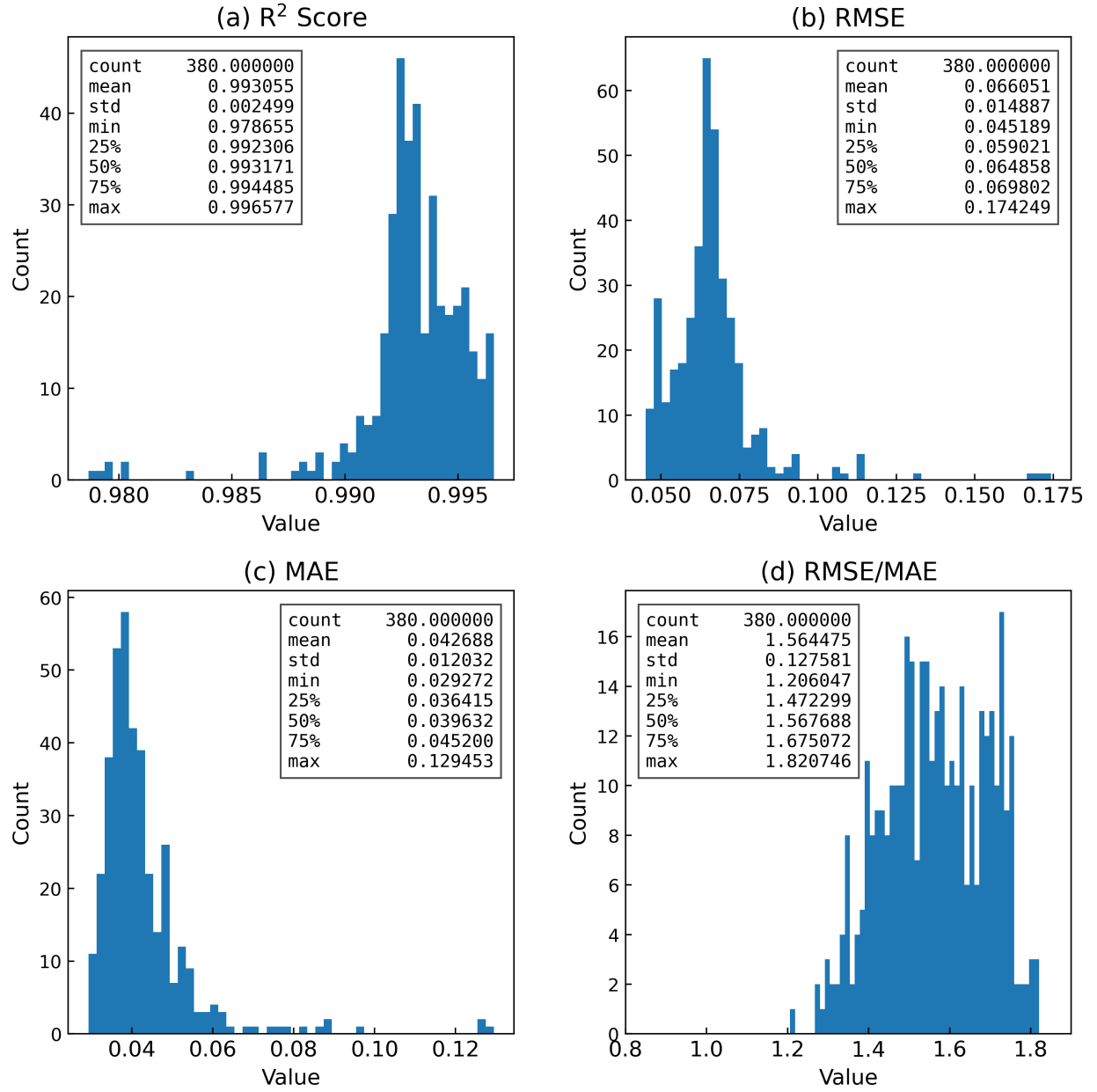


Figure 6: DeepONet model trained with the training data Set1. Each pane represents; (a)  $R^2$  score, (b) RMSE, (c) MAE, and (d) RMSE/MAE.

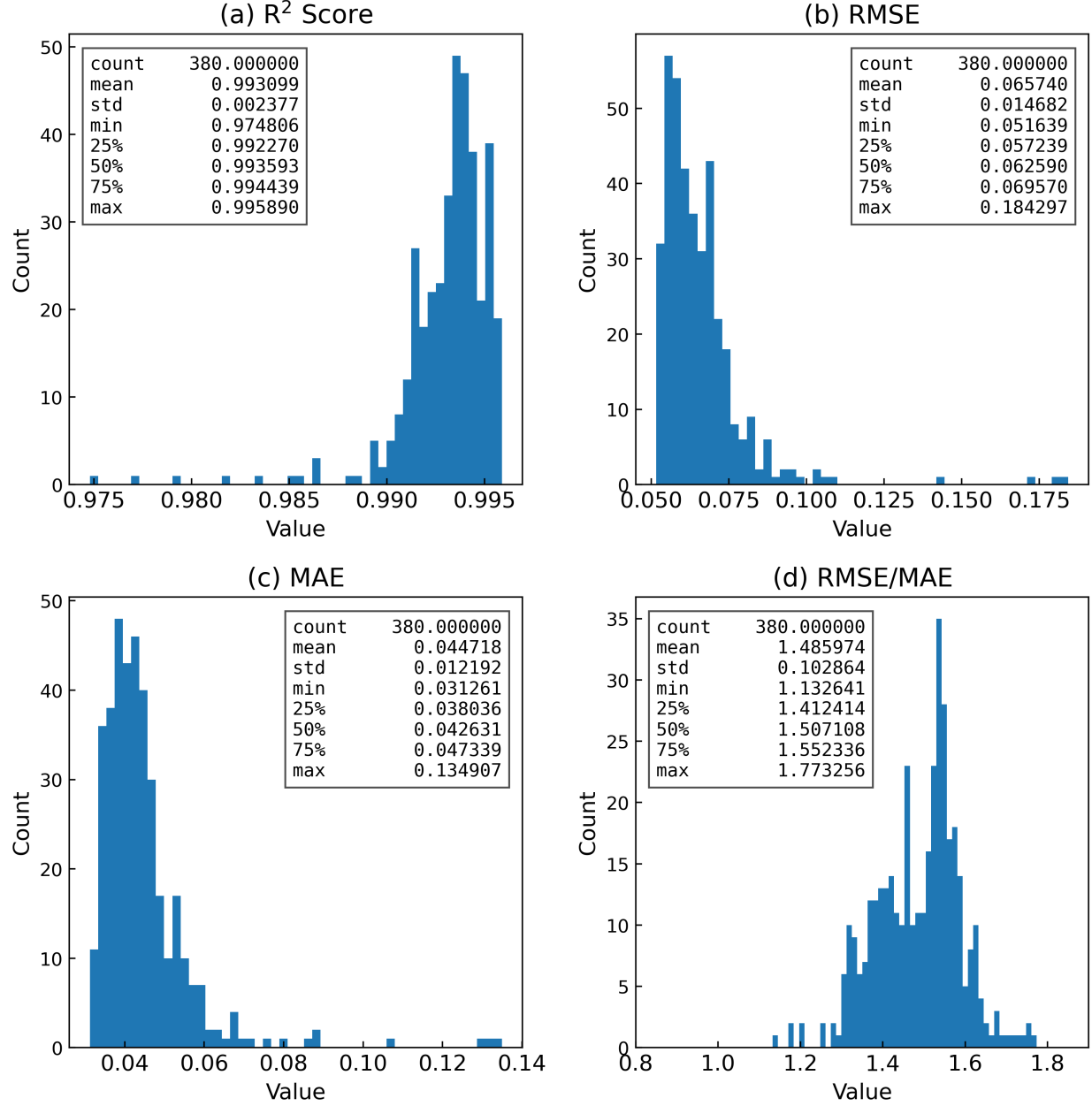


Figure 7: DeepONet model trained with the training data Set2. Each pane represents; (a)  $R^2$  score, (b) RMSE, (c) MAE, and (d) RMSE/MAE.

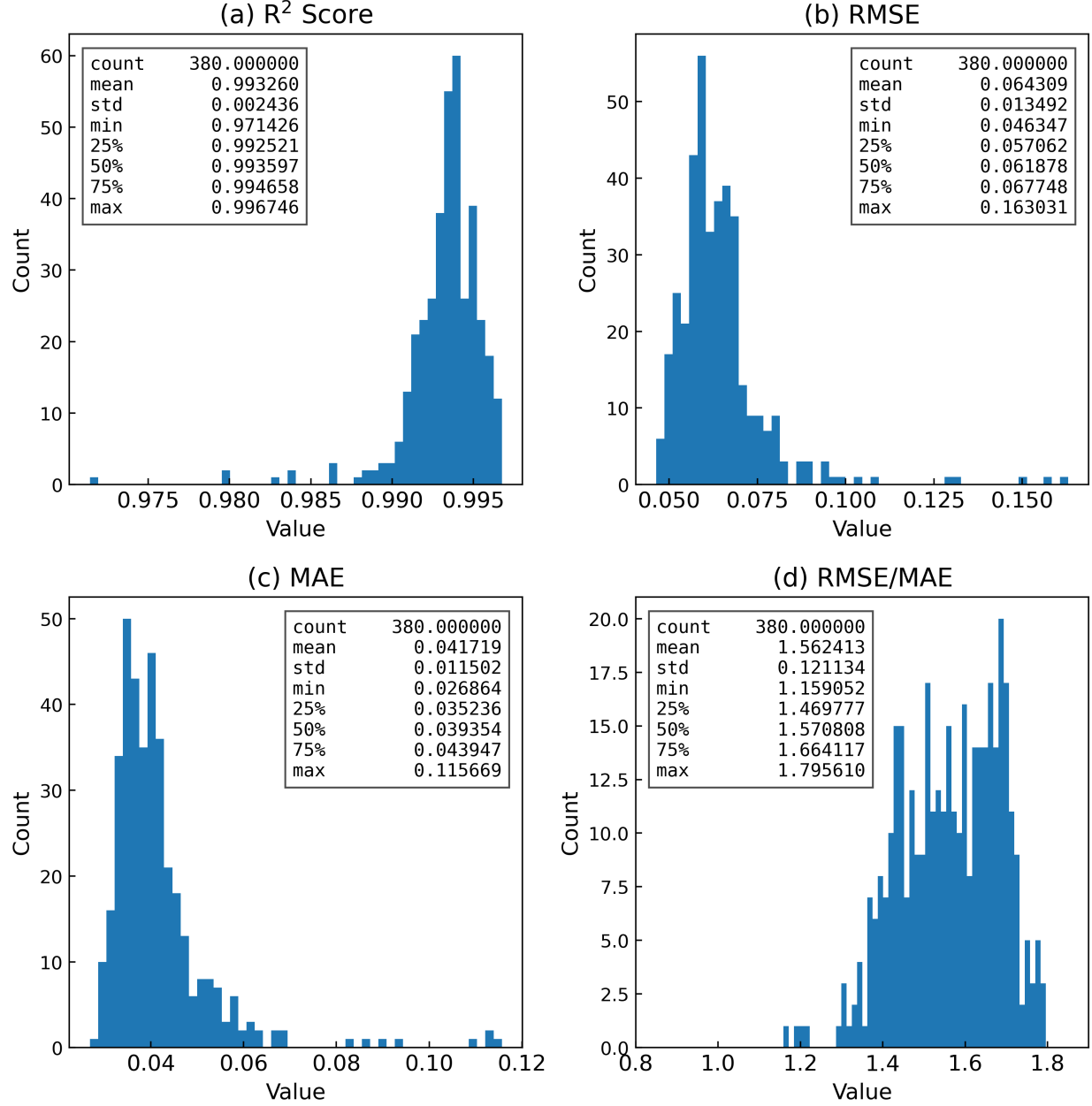


Figure 8: DeepONet model trained with the training data Set3. Each pane represents; (a)  $R^2$  score, (b) RMSE, (c) MAE, and (d) RMSE/MAE.

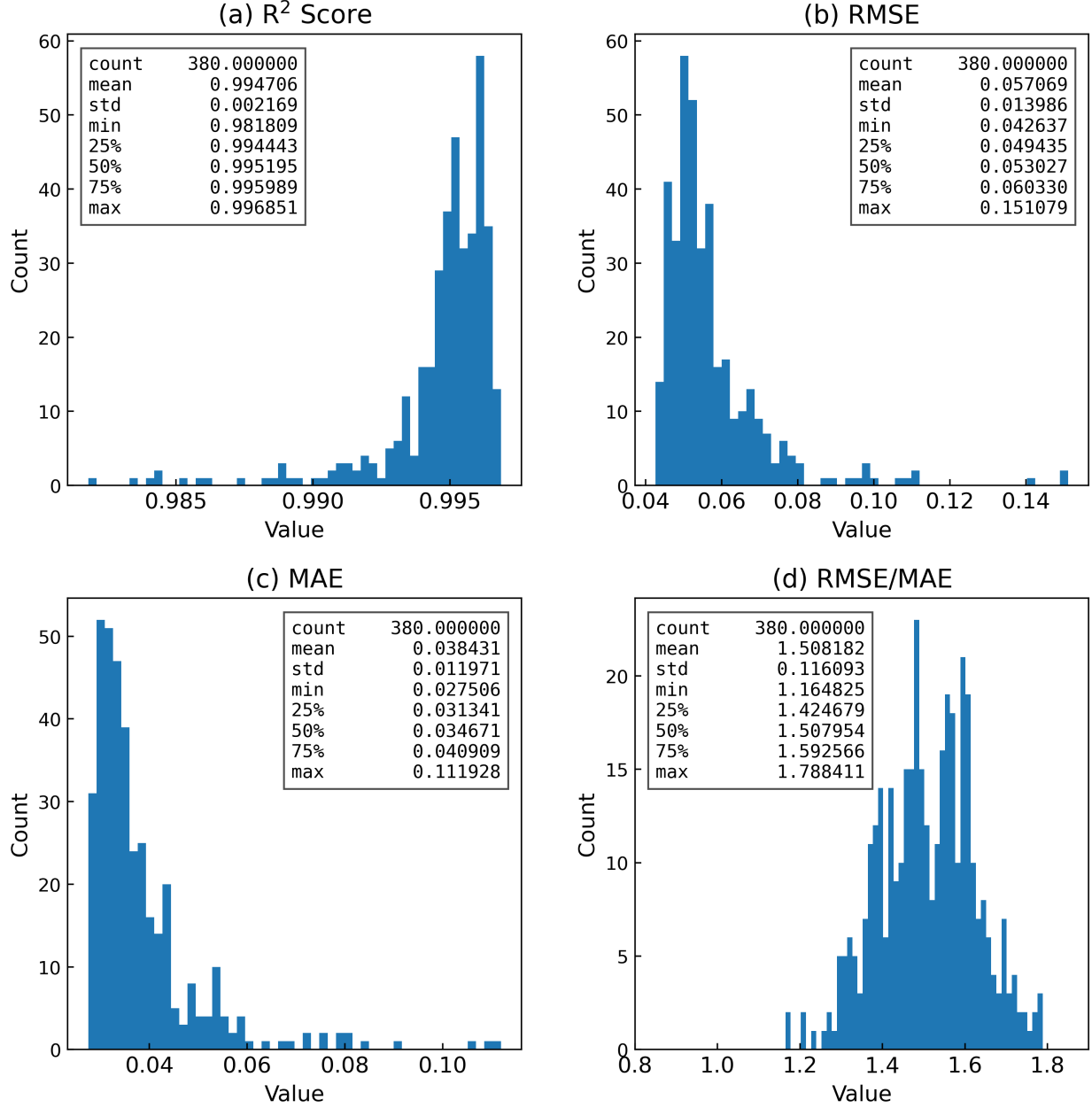


Figure 9: DeepONet model trained with the training data Set4. Each pane represents; (a)  $R^2$  score, (b) RMSE, (c) MAE, and (d) RMSE/MAE.

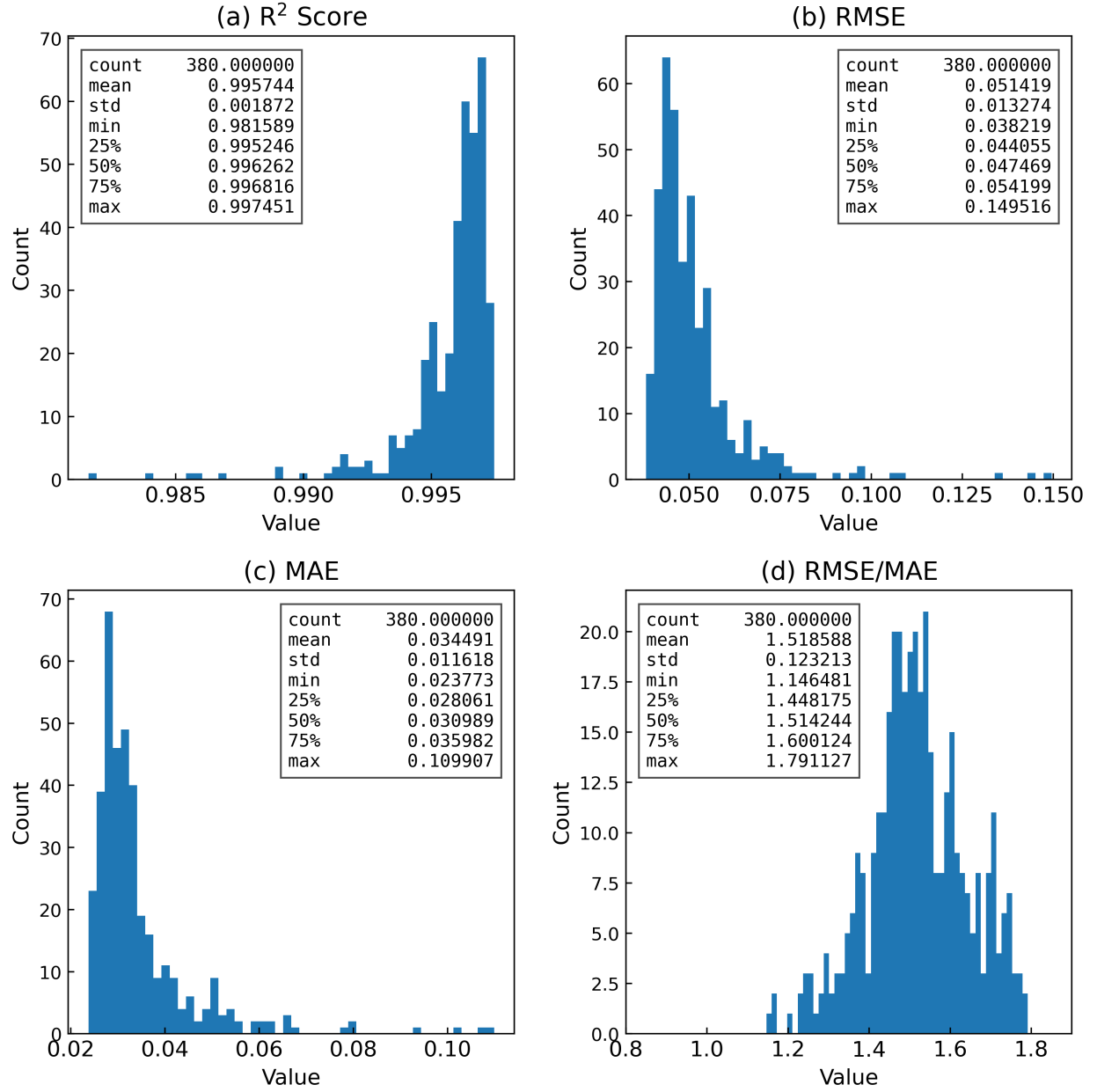


Figure 10: DeepONet model trained with the training data Set5. Each pane represents; (a)  $R^2$  score, (b) RMSE, (c) MAE, and (d) RMSE/MAE.



## C Network Architectures of FCN and CNN

In this study, we conducted a comprehensive comparison between DeepONet, and two conventional neural network methods: Fully-Connected Neural Networks (FCN) and Convolutional Neural Networks (CNN). All FCNs and CNNs were implemented using the PyTorch 2.0 deep learning framework, ensuring a standardized and efficient modeling process.

### C.1 FCN

The FCNs used in this study were constructed with a simple architecture consisting of an input layer, a hidden layer, and an output layer. The input layer had 2 neurons, the hidden layer contained 1024 neurons, and the output layer consisted of 1 neuron. ReLU activation functions were employed throughout the network. During training, the mean squared error (MSE) was used as the loss function, and the model parameters were optimized using the Adam optimization algorithm with a learning rate of 0.001. The training process utilized the mini-batch gradient descent method with a batch size of 20, iterated 1000 epochs.

```
FCN(
    (activation): ReLU()
    (linears): ModuleList(
      (0): Linear(in_features=2, out_features=1024, bias=True)
      (1): Linear(in_features=1024, out_features=1, bias=True)
    )
)
```

### C.2 CNN

CNNs were designed with a more complex architecture, including an input layer, a 1-dimensional convolutional layer, two linear layers, and an output layer. Dropout layers were incorporated with a dropout rate of 0.05 to prevent overfitting. The input and output layers each had 2 neurons, while the convolutional layer had 1 input channel and 1024 output channels with a kernel size of 1. Outputs from the convolutional layer were passed through linear layers, generating 2048 outputs before reaching the final output layer. Tanh activation functions were used in the network. The CNN model was also trained using MSE as the loss function, with the Adam optimization algorithm and a learning rate of 0.001. Training employed the mini-batch gradient descent method with a batch size of 50, repeated for 1000 epochs.

```
CNN(
    (activation): Tanh()
    (cnn1): Conv1d(1, 1024, kernel_size=(1,), stride=(1,))
    (flat): Flatten(start_dim=1, end_dim=-1)
    (dropout): Dropout(p=0.05, inplace=False)
    (lin1): Linear(in_features=2048, out_features=2048, bias=True)
    (lin2): Linear(in_features=2048, out_features=1, bias=True)
)
```

## References

- Vaibhav Yadav, Vivek Agarwal, Andrei V Gribok, Ross D Hays, Adam J Pluth, Christopher S Ritter, Hongbin Zhang, Prashant K Jain, Pradeep Ramuhalli, Doug Eskins, et al. Technical challenges and gaps in digital-twin-enabling technologies for nuclear reactor applications, 2021.
- Kazuma Kobayashi, Dinesh Kumar, Susmita Naskar, Souvik Chakraborty, Kyle Paaren, Joseph Graham, and Syed Alam. Non-intrusive uncertainty quantification for u3si2 and uo2 fuels with sic/sic cladding using bison for digital twin-enabling technology. *arXiv preprint arXiv:2211.13687*, 2022.
- Kobayashi Kazuma, James Daniell, Md Nazmus Sakib, Dinesh Kumar, and Syed Alam. Components of intelligent digital twin framework for complex nuclear systems. In *13th Nuclear Plant Instrumentation, Control & Human-Machine Interface Technologies (NPIC&HMIT 2023)*, 2023.
- IBM. What is a digital twin. <https://www.ibm.com/topics/what-is-a-digital-twin>. Accessed: 01.09.2023.
- Amazon Web Services. What is a digital twin. <https://aws.amazon.com/what-is/digital-twin/>. Accessed: 01.09.2023.

- GE Digital. Digital twin. <https://www.ge.com/digital/applications/digital-twin>. Accessed: 01.09.2023.
- Redshift by AUTODESK. What is a digital twin? how intelligent data models can shape the built world. <https://redshift.autodesk.com/articles/what-is-a-digital-twin>. Accessed: 01.09.2023.
- M Rahman, Abid Khan, Sayeed Anowar, Md Al-Imran, Richa Verma, Dinesh Kumar, Kazuma Kobayashi, and Syed Alam. Leveraging industry 4.0–deep learning, surrogate model and transfer learning with uncertainty quantification incorporated into digital twin for nuclear system. *Springer Nature Handbook of Smart Energy Systems, arXiv preprint arXiv:2210.00074*, 2022.
- James Daniell, Kazuma Kobayashi, Dinesh Kumar, Souvik Chakraborty, Ayodeji Alajo, Ethan Taber, Joseph Graham, and Syed Alam. Physics-informed multi-stage deep learning framework development for digital twin-centred state-based reactor power prediction. *arXiv preprint arXiv:2211.13157*, 2022.
- James Daniell, Kazuma Kobayashi, S. Chakraborty P. Bhowmik, and Syed Alam. Transfer learning technique using similar phenomena training for fuel digital twins of nuclear systems. In *13th Nuclear Plant Instrumentation, Control & Human-Machine Interface Technologies (NPIC&HMIT 2023)*, 2023.
- Kazuma Kobayashi, James Daniell, Dinesh Kumar, and Syed Alam. Role of operator learning in digital twin systems for energy systems. In *PSAM 2023 Topical Conference: AI & Risk Analysis for Probabilistic Safety Assessment and Management*, 2023a.
- Kazuma Kobayashi, James Daniell, and Syed B Alam. Neural operator framework for digital twin and complex engineering systems. *arXiv preprint arXiv:2301.06701*, 2023b.
- Lu Lu, Pengzhan Jin, Guofei Pang, Zhongqiang Zhang, and George Em Karniadakis. Learning nonlinear operators via deepnet based on the universal approximation theorem of operators. *Nature machine intelligence*, 3(3):218–229, 2021a.
- Tianping Chen and Hong Chen. Universal approximation to nonlinear operators by neural networks with arbitrary activation functions and its application to dynamical systems. *IEEE transactions on neural networks*, 6(4):911–917, 1995.
- Shengze Cai, Zhicheng Wang, Lu Lu, Tamer A. Zaki, and George Em Karniadakis. Deepm&mnet: Inferring the electroconvection multiphysics fields based on operator approximation by neural networks. *Journal of Computational Physics*, 436:110296, 2021. ISSN 0021-9991. doi:<https://doi.org/10.1016/j.jcp.2021.110296>. URL <https://www.sciencedirect.com/science/article/pii/S0021999121001911>.
- Lu Lu, Xuhui Meng, Zhiping Mao, and George Em Karniadakis. DeepXDE: A deep learning library for solving differential equations. *SIAM Review*, 63(1):208–228, 2021b. doi:10.1137/19M1274067.
- Somdatta Goswami, Minglang Yin, Yue Yu, and George Em Karniadakis. A physics-informed variational deepnet for predicting crack path in quasi-brittle materials. *Computer Methods in Applied Mechanics and Engineering*, 391:114587, 2022. ISSN 0045-7825. doi:<https://doi.org/10.1016/j.cma.2022.114587>. URL <https://www.sciencedirect.com/science/article/pii/S004578252200010X>.
- Tatsuhiko Sato, Yosuke Iwamoto, Shintaro Hashimoto, Tatsuhiko Ogawa, Takuya Furuta, Shin-ichiro Abe, Takeshi Kai, Pi-En Tsai, Norihiro Matsuda, Hiroshi Iwase, et al. Features of particle and heavy ion transport code system (phits) version 3.02. *Journal of Nuclear Science and Technology*, 55(6):684–690, 2018.
- Keiichi Shibata, Osamu Iwamoto, Tsuneo Nakagawa, Nobuyuki Iwamoto, Akira Ichihara, Satoshi Kunieda, Satoshi Chiba, Kazuyoshi Furutaka, Naohiko Otuka, Takaaki Ohsawa, et al. Jendl-4.0: a new library for nuclear science and engineering. *Journal of Nuclear Science and Technology*, 48(1):1–30, 2011.